Highly efficient and low hysteresis methylammonium-free perovskite solar cells based on multifunctional oteracil potassium interface modification

Huan Bi[1,2], Yao Guo[3], Mengna Guo[1], Chao Ding[2], Shuzi Hayase[2], Tao Mou[4], Qing Shen[2], Gaoyi Han[1]*, and Wenjing Hou[1]**

[1]Institute of Molecular Science, Key Laboratory of Materials for Energy Conversion and Storage of Shanxi Province, Shanxi University, Taiyuan 030006, P. R. China

[2]Faculty of Informatics and Engineering, The University of Electro-Communications, 1-5-1 Chofugaoka, Chofu, Tokyo 182-8585, Japan.

[3]School of Materials Science and Engineering, Henan Joint International Research Laboratory of Nanocomposite Sensing Materials, Anyang Institute of Technology, Anyang 455000, P. R. China

[4]Southwest Integrated Circuit Design Co., Ltd. Shapingba District, Chongqing, 401332, P. R. China

Corresponding Authors (Q. Shen, G. Han, W. Hou)

E-mail: shen@pc.uec.ac.jp

E-mail: han_gaoyis@sxu.edu.cn

E-mail: houwenjing@sxu.edu.cn

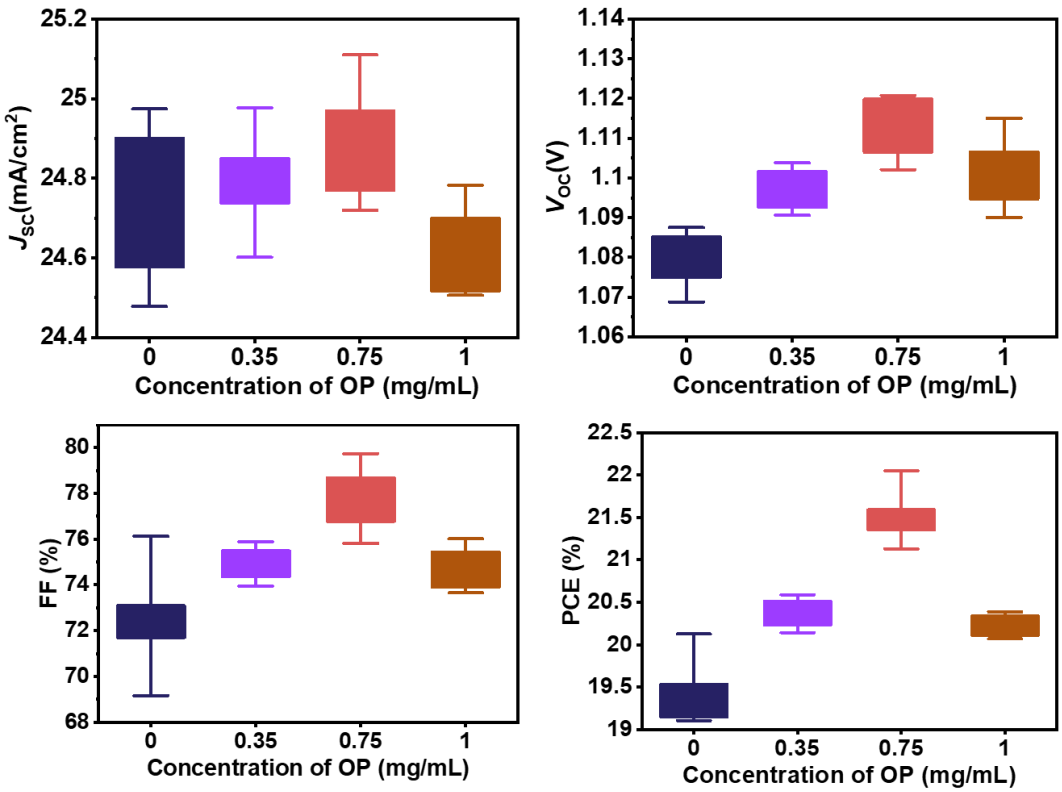

Fig. S1 Statistics of (a) J_{SC}, (b) V_{OC}, (c) FF, and (d) PCE of PSCs based on SnO_2 ETL modified by different concentrations of OP.

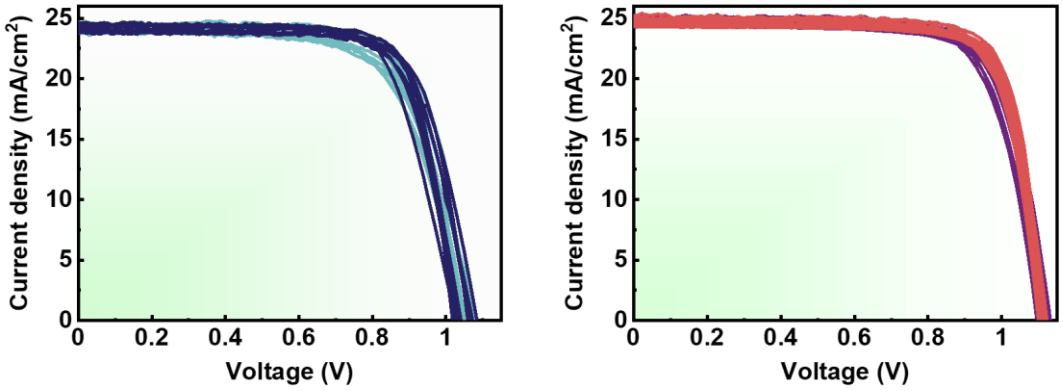

Fig. S2 *J-V* curves of the PSCs based on SnO_2 and SnO_2/OP (0.75 mg/mL).

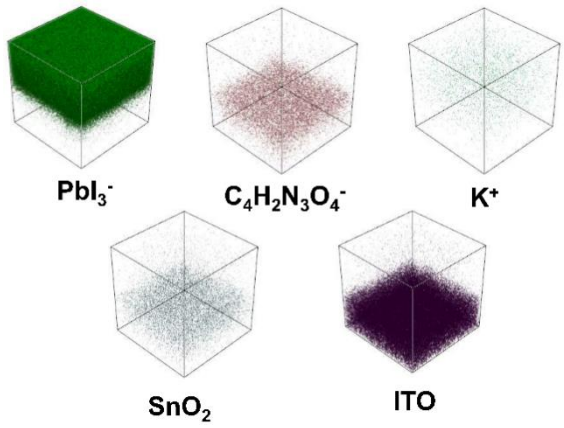

Fig. S3 Tof-SIMS 3D-depth profiles of the target devices with the structure of ITO/SnO_2/OP/perovskite. It needs to be noted that the chemical formula of OP is $C_4H_2N_3O_4K$. As shown in the Fig. S3, obvious boundaries can be observed in perovskite, OP, SnO_2, and ITO. In which, it can be seen that K^+ has diffused into perovskite layer in a gradient distribution and partially exists on the surface, which is consistent with the result of EDS.

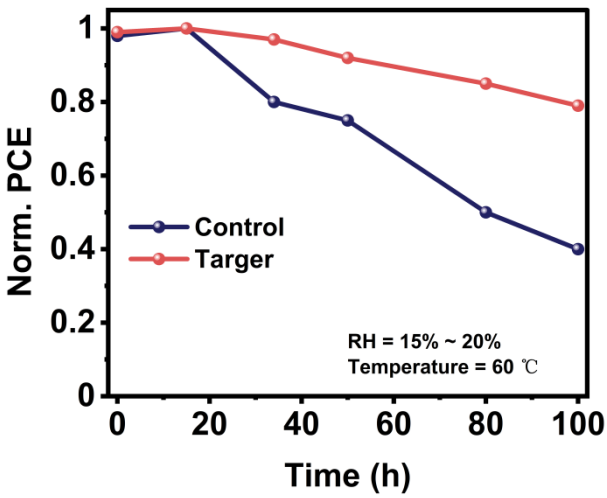

Fig. S4 PCE evolution of the unencapsulated control and target devices aged at 60 ℃ in dark conditions with the relative humidity of 15%-20%.

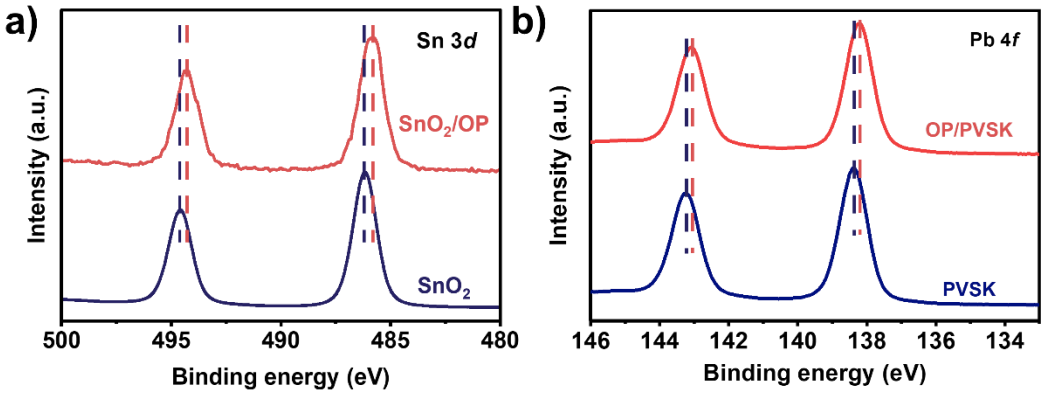

Fig. S5 XPS spectra of (a) Sn 3*d* of SnO_2 and SnO_2/OP films; (b) Pb 4*f* of perovskite and OP/perovskite film.

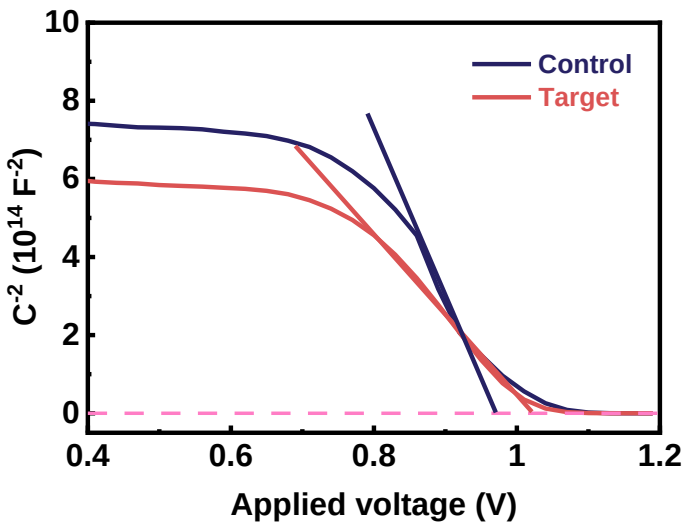

Fig. S6 Mott-Schottky plot of the control and target devices.

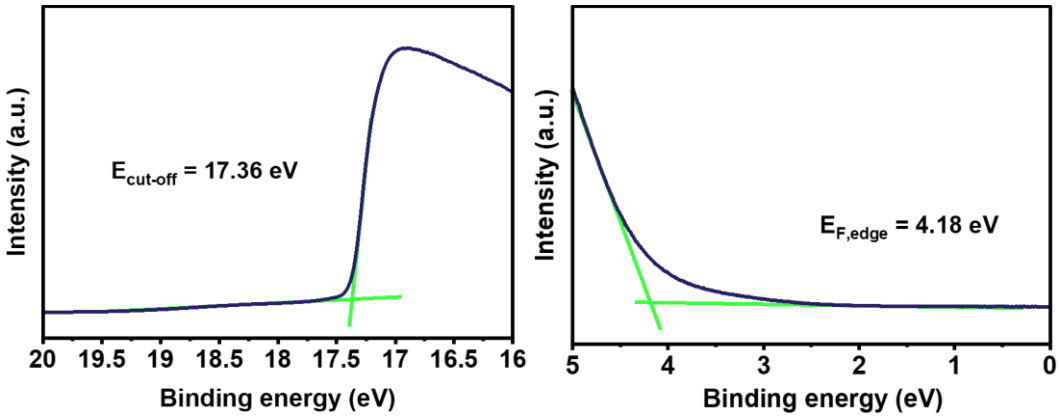

Fig. S7 The cut-off energy (E_{cut}-off) and Fermi edge (E_F) of the SnO_2 film.

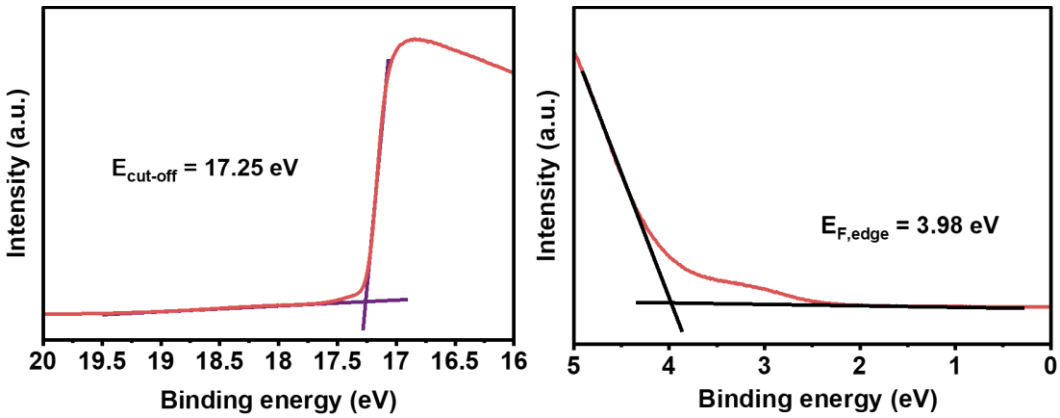

Fig. S8 The cut-off energy (E_{cut}-off) and Fermi edge (E_F, edge) of the SnO_2 film modified by OP.

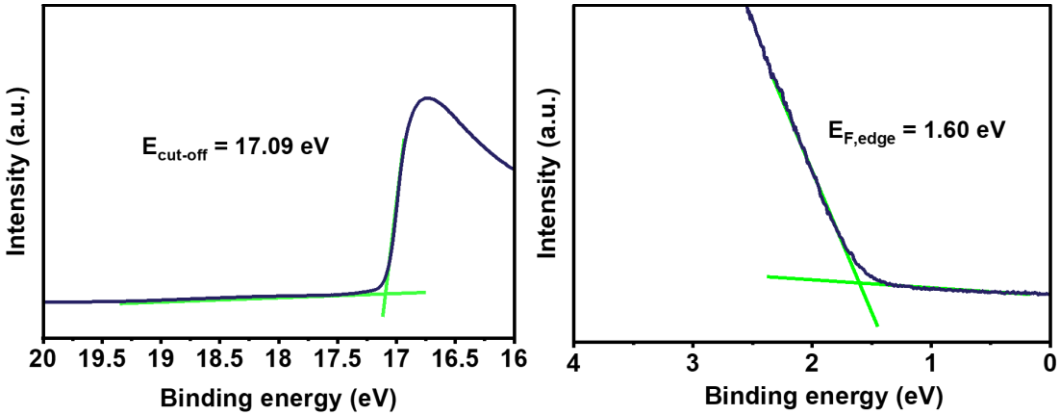

Fig. S9 The cut-off energy (E_{cut}-off) and Fermi edge (E_F, edge) of the perovskite film.

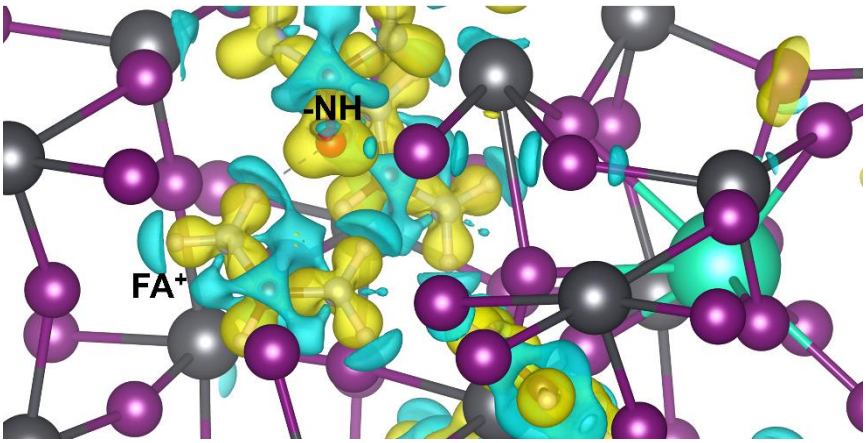

Fig. S10 The charge density difference of -NH (in OP) and FA^+ (in perovskite).

Table S1. Champion and average photovoltaic parameters of the PSCs modified different concentrations of OP.

OP (mg/mL)		J_{SC} (mA/cm^2)	V_{OC} (V)	FF	PCE (%)
	Champion	**24.41**	**1.08**	**76.12**	**20.07**
0	Average	24.74	1.08	73.73	19.70
	Std. Dev.	0.193	0.007	1.493	0.430
	Champion	**24.77**	**1.10**	**75.53**	**20.58**
0.35	Average	24.79	1.09	75.48	20.39
	Std. Dev.	0.102	0.005	0.609	0.144
	Champion	**24.82**	**1.12**	**79.48**	**22.09**
0.75	Average	24.88	1.12	77.78	21.67
	Std. Dev.	0.120	0.007	1.343	0.241
	Champion	**24.64**	**1.09**	**75.80**	**20.35**
1	Average	24.62	1.08	75.48	20.06
	Std. Dev.	0.097	0.007	0.798	0.120

Table S2. Summary of photovoltaic performance of reported high-efficiency FACs-based PSCs to date.

Device structure	J_{SC} (mA/cm^2)	V_{OC} (V)	FF	PCE (%)	Active area (cm^2)	Ref.
ITO/SnO_2/OP/$Rb_{0.02}(FA_{0.95}Cs_{0.05})_{0.98}PbI_{2.91}Br_{0.03}Cl_{0.06}$/Spiro-OMeTAD/Au	**24.82**	**1.120**	**0.795**	**22.09**	**0.1**	**This work**
ITO/SnO_2/$Rb_{0.02}(FA_{0.95}Cs_{0.05})_{0.98}PbI_{2.91}Br_{0.03}Cl_{0.06}$/Spiro-OMeTAD/Ag	22.97	1.160	0.822	21.92	0.07	[S1]
ITO/SnO_2/$Rb_{0.02}(FA_{0.95}Cs_{0.05})_{0.98}PbI_{2.91}Br_{0.03}Cl_{0.06}$/Spiro-OMeTAD/Ag	23.18	1.163	0.825	22.22	0.07	[S2]
ITO/SnO_2/ZnO/ $FA_{0.95}Cs_{0.05}PbI_3$/ Spiro-OMeTAD/Ag	24.35	1.126	0.784	21.50	0.06	[S3]
ITO/ZnO/SnO_2/$FA_{0.9}Cs_{0.1}PbI_3$/ Spiro-OMeTAD /MoO_3/Ag	24.60	1.090	0.773	20.70	NO	[S4]
TFO/cp-TiO_2/mp-TiO_2/SnO_2/$(Cs_{0.17}FA_{0.83})Pb(I_{0.89}Br_{0.08}Cl_{0.03})_3$/ Spiro-OMeTAD/Au	23.28	1.120	0.783	20.50	0.1	[S5]
FTO/c-TiO_2/$(Cs_{0.2}FA_{0.8})Pb(I_{0.95}Br_{0.05})_3$/Spiro-OMeTAD/Au	22.82	1.115	0.788	20.05	0.09	[S6]
FTO/c-TiO_2/mp-TiO_2/$FA_{0.9}Cs_{0.1}PbI_3$/Spiro-OMeTAD/Au	24.0	1.15	0.75	20.9	1.0	[S7]
FTO/SnO_2/PCBM@PMMA/$Rb_{0.05}Cs_{0.1}FAPbI_3$/Spiro-OMeTAD/Au	25.06	1.08	0.755	20.44	0.1024	[S8]
FTO/c-TiO_2/mp-TiO_2/$Cs_{0.20}FA_{0.80}PbI_3$/Spiro-OMeTAD/Au	24.10	1.10	0.776	20.60	0.16	[S9]
FTO/ZnO/$FA_{0.83}Cs_{0.17}PbI_{2.49}Br_{0.51}$/Spiro-OMeTAD/Au	22.5	1.2	0.781	21.1	0.0919	[S10]
FTO/c-TiO_2/mp-TiO_2/$Cs_{0.05}FA_{0.95}PbI_{3-x}Br_x$/Spiro-OMeTAD/Au	24.52	1.145	0.775	21.78	0.12	[S11]
FTO/c-TiO_2/$Cs_{0.15}FA_{0.85}PbI_{2.7}Br_{0.3}$/Spiro-OMeTAD/Au	22.57	1.179	0.801	21.30	0.09	[S12]
ITO/PTAA/PFN-Br/$FA_{0.83}Cs_{0.17}PbI_{2.4}Br_{0.6}$/ C_{60}/BCP/Ag	22.58	1.15	0.81	21.11	0.1	[S13]
FTO/c-TiO_2/$Cs_{0.15}FA_{0.85}PbI_{2.7}Br_{0.3}$/Spiro-OMeTAD/Au	23.06	1.146	0.798	21.07	0.09	[S14]

Table S3. Fitted results of TRPL dynamics of the perovskite films deposited on the Glass and Glass/OP.

	Glass/PVSK	**Glass/OP/PVSK**
τ_1 (ns)	16.50	23.08
%	96.81	94.09
τ_2 (ns)	45.55	105.69
%	3.19	6.28
τ_{ave} (ns)	18.92	42.41

Table S4. Fitted results of TRPL curves of the perovskite films deposited on the different substrates with SnO_2 or with SnO_2/OP.

	ITO/SnO_2/PVSK	**ITO/SnO_2/OP/PVSK**
τ_1 (ns)	5.12	2.70
%	0.79	0.88
τ_2 (ns)	11.12	9.25
%	0.21	0.12
τ_{ave} (ns)	7.39	4.78

References

[S1] B. Liu, H. Bi, D. He, L. Bai, W. Wang, H. Yuan, Q. Song, P. Su, Z. Zang, T. Zhou, J. Chen, Interfacial defect passivation and stress release via multi-active-site ligand anchoring enables efficient and stable methylammonium-free perovskite solar cells, ACS Energy Lett. 6 (2021) 2526-2538.

[S2] X. Zuo, B. Kim, B. Liu, D. He, L. Bai, W. Wang, C. Xu, Q. Song, C. Jia, Z. Zang, D. Lee, X. Li, J. Chen, Passivating buried interface via self-assembled novel sulfonium salt toward stable and efficient perovskite solar cells, Chem. Eng. J. 431 (2021) 133209.

[S3] Q. Yao, Q. Xue, Z. Li, K. Zhang, T. Zhang, N. Li, S. Yang, C.J. Brabec, H.-L. Yip, Y. Cao, Graded 2D/3Dperovskite heterostructure for efficient and operationally stable MA-free perovskite solar cells, Adv. Mater. 32 (2020) 2000571.

[S4] L. Yan, Z. Li, T. Niu, X. Xu, S. Xie, G. Dong, Q. Xue, H.-L. Yip, Effects of ZnI_2 doping on the performance of methylammonium-free perovskite solar cells, J. Appl. Phys. 128 (2020) 043102.

[S5] X.X. Gao, W. Luo, Y. Zhang, R. Hu, B. Zhang, A. Zuttel, Y. Feng, M.K. Nazeeruddin, Stable and high-efficiency methylammonium-free perovskite solar cells, Adv. Mater. 32 (2020) e1905502.

[S6] Y. Wu, P. Wang, S. Wang, Z. Wang, B. Cai, X. Zheng, Y. Chen, N. Yuan, J. Ding, W.-H. Zhang, Heterojunction engineering for high efficiency cesium formamidinium double-cation lead halide perovskite solar cells, ChemSusChem 11 (2018) 837-842.

[S7] D. Bi, X. Li, J.V. Milić, D.J. Kubicki, N. Pellet, J. Luo, T. LaGrange, P. Mettraux, L. Emsley, S.M. Zakeeruddin, M. Grätzel, Multifunctional molecular modulators for perovskite solar cells with over 20% efficiency and high operational stability, Nat. Commun. 9 (2018) 4482.

[S8] S.-H. Turren-Cruz, A. Hagfeldt, M. Saliba, Methylammonium-free, high-performance, and stable perovskite solar cells on a planar architecture, Science 362 (2018) 449.

[S9] D. Prochowicz, R. Runjhun, M.M. Tavakoli, P. Yadav, M. Saski, A.Q. Alanazi, D.J. Kubicki, Z. Kaszkur, S.M. Zakeeruddin, J. Lewiński, M. Grätzel, Engineering of perovskite materials based on formamidinium and cesium hybridization for high-efficiency solar cells, Chem. Mater. 31 (2019) 1620-1627.

[S10] K. Schutt, P.K. Nayak, A.J. Ramadan, B. Wenger, Y.-H. Lin, H.J. Snaith, Overcoming zinc oxide interface instability with a methylammonium-free perovskite for high-performance solar cells, Adv. Funct. Mater. 29 (2019) 1900466.

[S11] L. Xie, K. Lin, J. Lu, W. Feng, P. Song, C. Yan, K. Liu, L. Shen, C. Tian, Z. Wei, Efficient and stable low-bandgap perovskite solar cells enabled by a $CsPbBr_3$-cluster assisted bottom-up crystallization approach, J. Am. Chem. Soc. 141 (2019) 20537-20546.

[S12] J. Yang, Y. Chen, W. Tang, S. Wang, Q. Ma, Y. Wu, N. Yuan, J. Ding, W.-H. Zhang, Crystallization tailoring of cesium/formamidinium double-cation perovskite for efficient and highly stable solar cells, Journal of Energy Chemistry 48 (2020) 217-225.

[S13] S. Li, K. Fan, Y. Cui, S. Leng, Y. Ying, W. Zou, Z. Liu, C.-Z. Li, K. Yao, H. Huang, Unravelling the mechanism of ionic fullerene passivation for efficient and stable methylammonium-free perovskite solar cells, ACS Energy Lett. 5 (2020) 2015-2022.

[S14] Y. Chen, J. Yang, S. Wang, Y. Wu, N. Yuan, W.-H. Zhang, Interfacial contact passivation for efficient and stable cesium-formamidinium double-cation lead halide perovskite solar cells, iScience 23 (2020) 100762.